Communication

Sparse-Array Metasurface for Beam Scanning

Jonathan Dessy, Modeste Bodehou, Jean Cavillot, and Christophe Craeye

***Abstract*— Beam scanning is traditionally achieved with phased arrays, whose application often faces the challenge of high density of antennas and associated electronic components. Metasurfaces (MTS) allow the tailoring of pencil and shaped beams with a low-profile radiator, but scanning with MTSs remains difficult, e.g., reconfiguring each subwavelength patch of the MTS defeats the initial purpose of simplicity. This communication proposes a novel design approach to beam scanning with surface-wave (SW)-based MTS antennas. Both the feeding and the MTS are made periodic at a scale of a few wavelengths. To avoid grating lobes, the unit cell of the periodic MTS is designed, such that the embedded element pattern (EEP) has a nearly rectangular shape with proper width. The sparsity of the feeding system enables a drastic reduction of the density of electronics at the expense of a smaller field of view. The resulting antenna, demonstrated here in 2-D (uniform antenna versus one space coordinate), has low profile (including the feeder) and enables continuous beam scanning with high gain. With a spacing of two wavelengths between feeds, the scan range is +/−10°. The MTS is first designed at the surface impedance level, and the resulting structure has then been validated through full-wave simulation of a MTS implemented with subwavelength patches. Numerical analysis versus frequency indicates a pattern bandwidth of the order of 5%.**

***Index Terms*— Beam scanning, embedded element pattern (EEP), metasurface (MTS), periodic method of moments (MoM), sparse array.**

I. Introduction

Surface-wave (SW)-based metasurface (MTS) antennas are typically realized with a grounded dielectric slab on which dense subwavelength metal patterns of varying shape, size, and orientation are periodically printed [1], [2], [3]. The antenna plane includes an integrated feeder that generates SWs within the dielectric slab. The SW is progressively perturbed by a smooth spatial variation of the shape of the patches. That perturbation generates leaky waves, potentially producing a well-controlled radiation pattern [4], [5]. The metallization layer can reliably be modeled as a spatially modulated sheet impedance lying on the grounded slab [6], [7], [8], [9].

SW-based MTS antennas can be designed to achieve multiple beams [10], [11], but continuous beam scanning remains a great challenge with this technology. The first and probably most popular approach to scan the beam with MTSs consists of tuning or switching each individual printed patch [12], [13]. However, considering the high number of unit cells, this approach requires an extremely dense controlling circuit, such that the main advantage over phased arrays, i.e., sparsity of the electronic circuits, is lost. A second method makes use of tunable dielectric materials, such as liquid crystals [14], but those are in general quite lossy and the electronics may become complex for a local control of the dielectric slab permittivity. A third approach has been proposed in [11] by combining two patterns with opposite phase slopes, created with widely separated feeds. However, the beam scanning capability of this technique is limited to one beamwidth.

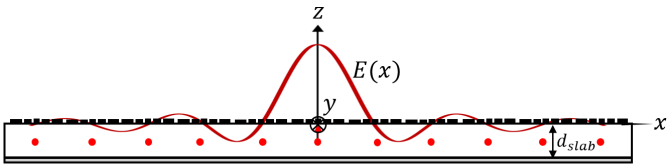

Fig. 1. $\sin(x)/x$ shape of the electric field contributing to radiation for excitation of the center feed.

On the other hand, phased arrays are a famous and mature technology offering an excellent beam controllability. However, it is well known that phased arrays require a maximum spacing of half-wavelength (up to one wavelength in case of limited scan range) between active elements to avoid grating lobes, resulting in a dense electronic front end [15]. Sparse phased array systems (i.e., with spacing larger than half-wavelength) with rectangular embedded element pattern (EEP) able to cut the grating lobes have been proposed in the literature [16], [17]. It can be shown that such sharp patterns necessarily result from wide field distributions, which have a $\sin(x)/x$ shape. Consequently, currents and fields due to different feeds must overlap over multiple array cells to occupy the entire array aperture [18], [19], as illustrated in Fig. 1. To meet this constraint, different solutions have already been investigated in the literature. Initially, tapered waveguide arrays were proposed to target this kind of current distribution along the antenna [17]. However, such structures are very bulky, and performance is limited, because no overlapping of the fields over the antenna is possible. A technique called overlapped subarrays can solve this issue by enabling the overlapping of the fields along the structure. The most general approach to form overlapped subarrays consists of applying multiport beamforming networks arranged between control devices and radiating elements, such as the Shelton's [20] network made with two cascaded Butler matrices [21], [22]. These overlapped subarray networks provide good pattern control at the expense of an increased complexity. Other architectures for overlapped subarrays based on waveguides are described in [19], [21], [23], and [16], with the disadvantage of being bulky. Solutions based on superstrate lenses [24], [25] or transmit arrays [26] have also been envisaged. However, the antenna, including its feeding system, is significantly thick. Therefore, there is a need of low-profile antennas with high gain

Manuscript received 21 December 2023; revised 14 June 2024; accepted 31 July 2024. Date of publication 13 August 2024; date of current version 8 October 2024. This work was supported in part by the Research Fellow Aspirant (ASP) grant through Belgium Fonds National de la Recherche Scientifique (F.R.S.-FNRS); in part by European FITNESS Pathfinder Project under Grant 101098996; in part by Computational Resources that have been provided by the Supercomputing Facilities, Université catholique de Louvain (CISM/UCL); and in part by the Consortium des Équipements de Calcul Intensif en Fédération Wallonie Brussels (CÉCI) funded by the Fond de la Recherche Scientifique de Belgique (F.R.S.-FNRS) and by the Walloon Region under Grant 2.5020.11. *(Corresponding author: Jonathan Dessy.)*

Jonathan Dessy, Jean Cavillot, and Christophe Craeye are with the ICTEAM Institute, Université catholique de Louvain (UCLouvain), 1348 Louvain-la-Neuve, Belgium (e-mail: jonathan.dessy@uclouvain.be; jean.cavillot@uclouvain.be; christophe.craeye@uclouvain.be).

Modeste Bodehou is with the Ecole Polytechnique d'Abomey-Calavi, Université d'Abomey-Calavi (UAC), Cotonou, Benin (e-mail: modeste.bodehou@gmail.com).

Digital Object Identifier 10.1109/TAP.2024.3439776

and capable of beam scanning with relatively few active elements as compared with traditional phased arrays. This type of antennas can be used in applications requiring a limited field of view with cheap hardware, such as sectoral base stations [27], spotlight synthetic aperture radar (SAR) [28], detection, and surveillance over limited areas.

The goal of this communication is to propose and to show that the required sharp EEP can be produced with a sparse-array MTS, as the current induced by each excitation can naturally propagate over the whole structure and, thus, overlap the currents generated by the other feeding points. In other words, array-fed MTS antennas offer the possibility to target sharp EPPs, as the shared dielectric layer enables the propagation and overlapping of wide field distributions, which would not be possible with a discrete array of antennas. The structure consists of a smooth MTS aperture and fully takes advantage of the mutual coupling between patches along the MTS structure. Simulations of the proposed structure are carried out to provide a design of the MTS and support the feasibility of the concept idea, but the practical implementation of the antenna and its feeding network is beyond the scope of this communication. The reduced number of active feeds, and hence of electronic channels, results in an antenna that combines the advantages of phased arrays (reconfigurability), with those of MTSs (low-power losses, low profile, low cost, and simplicity of fabrication), while offering a high gain.

The remainder of this communication is structured as follows. Section II describes the considered MTS antenna structure and presents the tools for its analysis. Section III describes the consecutive steps toward the design of the surface impedance as well as the feeding required to obtain a nearly ideal EEP. A full-wave simulation of the surface impedance is carried out to validate the optimized design. Section IV evaluates the impact of array truncation, along with the bandwidth of the MTS antenna implemented with printed patches. Conclusions are drawn in Section V.

II. Analysis of 1-D Periodic MTS Antennas

The analysis as well as the designs provided in this communication are carried out in two dimensions (2-D problem) in order to highlight the fundamental principles on a simplified version of the problem. The work can then be extended to the analysis of 3-D problems with scanning in elevation and azimuth. In a classical Cartesian system of coordinates, the considered antenna is oriented along the x-direction and translationally invariant along the y-direction (see Fig. 1). This type of MTS will be named 1-D MTS. It consists of a MTS array, modeled as a sheet impedance printed on a grounded dielectric slab with relative permittivity ϵ_r and thickness d_{slab}. The sheet impedance is made periodic with period equal to the array cell size a. The antenna is excited with a SW launcher invariant along y. In this communication, the launcher is modeled as a vertical elementary dipole (VED) wall (along y) placed at the center of each cell and in the middle of the substrate ($z = -d_{slab}/2$). The VED model has been proven to be accurate in predicting the radiation pattern of SW-based MTS antennas [4], [29]. The excitations are all of the same amplitude but carry a phase shift $-\psi$ between consecutive array cells, as illustrated in Fig. 2, where the reference cell and the corresponding reference feed are highlighted in red.

An analysis of infinitely periodic structures with the method of moments (MoM) has been widely studied in the literature [30], [31]. In this type of problems, the discretization of the relevant unknown (the current distribution) can be limited to one array cell, called the reference cell, while explicitly enforcing periodic boundary conditions. As we assume a structure invariant along y, the analysis can be carried out in one dimension. Moreover, a purely transverse magnetic (TM) source with respect to the z-direction with isotropic

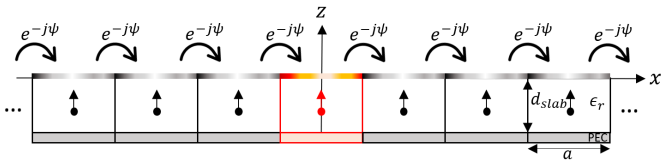

Fig. 2. 1-D infinite periodic MTS antenna, where the reference cell and the corresponding reference feed are highlighted in red.

MTS $Z_s(x)$ is considered for simplicity. Therefore, the current distribution and the tangential electric field on the aperture are oriented along the x-direction. To effectively discretize the current distribution, we used, in this communication, Gaussian basis functions as done, for example, in [7] for the analysis of finite MTSs. Each basis function F_b^n is defined as follows:

$$F_b^n(x) = \frac{1}{\sigma\sqrt{2\pi}} e^{\frac{-(x-\mu_n)^2}{2\sigma^2}} \tag{1}$$

where σ and μ_n are the standard deviation and the mean of the nth Gaussian function, respectively. Then, the periodic MoM equations can be formulated to efficiently compute the current distribution, as detailed in [32]. Once the current distribution is computed, the x-directed spectral electric field on the aperture $\tilde{E}_x$ is derived. For the considered 2-D problem, it can be shown that, in the far-field, the electric field $\boldsymbol{E}$ and the resulting EEP $\boldsymbol{F}$ can be obtained as follows:

$$\boldsymbol{E}(R,\theta) = \frac{e^{-jk_0R}}{\sqrt{R}} \underbrace{\left(-\sqrt{\frac{j}{\lambda}}\tilde{E}_x(\theta)\big(\sin\theta\hat{\boldsymbol{z}} - \cos\theta\hat{\boldsymbol{x}}\big)\right)}_{\boldsymbol{F}(\theta)\ [\mathrm{V}/\sqrt{\mathrm{m}}]} \quad [\mathrm{V/m}] \tag{2}$$

with (R,θ) being the classical polar system of coordinates ($(x,z) = (R\sin\theta, R\cos\theta)$) and $k_0 = 2\pi/\lambda$ is the free-space wavenumber, with λ the free-space wavelength. Finally, the 2-D directivity can be derived as follows:

$$D(\theta) = \frac{\pi|\boldsymbol{F}(\theta)|^2}{\eta P_{rad}} \quad [-] \tag{3}$$

where $\eta \approx 376.7\ \Omega$ is the free-space impedance and P_{rad} corresponds to the total power radiated by the MTS antenna per unit length along y and is given by

$$P_{rad} = \frac{1}{2\eta}\int_{\frac{-\pi}{2}}^{\frac{\pi}{2}} |\boldsymbol{F}(\theta)|^2 d\theta \quad [\mathrm{W/m}]. \tag{4}$$

Well-know results from the literature have been efficiently reproduced with the presented MoM formulation in [32].

III. Design of 1-D Periodic MTS Antennas

A. Ideal EEP

As explained in the introduction, we are looking for a sparse-array MTS able to generate the rectangular EEP required to cut the grating lobes of the array factor (see Fig. 3), taking into account the effect of the array of excited elements. The EEP must be centered on $\theta = 0°$ to enable symmetric beam scanning. Such a sparse-array MTS will be able to scan with significantly fewer active elements as compared with phased arrays. As a consequence, the electronics will be less complex, cheaper, and lighter. Of course, those benefits come with a reduction of the field of view. The latter is given by [18], [19]

$$|\theta_{max}| = \arcsin\left(\frac{\pi}{ak_0}\right) \tag{5}$$

where θ_{max} is the maximum allowed elevation angle consistent with the array cell size a. In the following, we consider a dielectric slab with relative permittivity $\epsilon_r = 3.66$ and thickness $d_{slab} = 1.524$ mm.

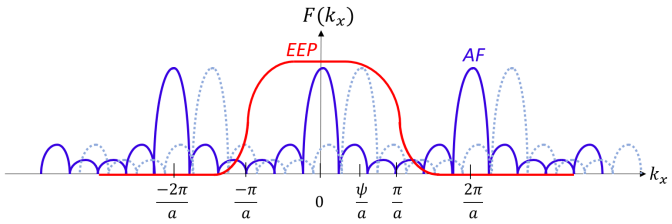

Fig. 3. Sharp filtering of the grating lobes of the array factor (AF, dashed with scanning) by the EEP, along the spectral coordinate k_x. The array has a feed spacing a and a phase shift $-\psi$ between consecutive elements.

The MTS is operating at 24 GHz with cell size $a = 2\lambda$. That would increase the feed spacing by a factor of 4 (in 1-D), while still allowing a scanning range of the order of about 28.96°. This range is very convenient for many applications, such as car traffic radars, sectoral base station antennas, and spotlight SAR.

B. First MTS Design Approach

We know that the unknown surface impedance should be purely imaginary in the absence of losses and ideally capacitive to facilitate the implementation with subwavelength printed patches [4], [33]. It should also be periodic at the scale of the array cell $a = 2\lambda$, in a regular array. Given the excitation source, the impressed impedance should not be symmetrical versus x, because this symmetry imposes a zero radiation at broadside. Finally, as explained in Oliner's paper [34], the periodicity of the modulation dictates the radiation angle. Considering all these constraints, we propose a capacitive impedance with a periodicity that evolves linearly along x, so that the covered range of periodicity allows one to spread the beam over the entire radiation sector dictated by the desired rectangular EEP (i.e., $k_0|\sin\theta| \leq \pi/a$), while ensuring a nonsymmetric reactance versus x. This impedance is given by

$$Z_s(x) = jX_0\left(1 + M\sin\left(2\pi\left(\pm\frac{f_2 - f_1}{a}x^2 + f_2 x\right)\right)\right) \quad (6)$$

on the reference cell, where the "+" sign is used for the negative space coordinates ($-a/2 \leq x < 0$) and the "−" sign is used for the positive space coordinates ($0 \leq x \leq a/2$). $X_0 = -772.5\ \Omega$ is the average reactance, $M = 0.95$ is the modulation depth, and f_1 and f_2 are the spatial modulation frequencies at the edges and the center of the cell, respectively. Targeting the ideal EEP requires that

$$f_{1,2} = \frac{k_{sw} - k_0\sin\left(\theta_{p1,2}\right)}{2\pi} \quad (7)$$

where $\theta_{p1} = -14.48°$ and $\theta_{p2} = 0°$ are the limits of the desired radiation sector, and $k_{sw} = 1.35\,k_0$ corresponds to the supported SW wavenumber in absence of modulation. Finally, the impedance is decomposed into Fourier series with 31 coefficients so as to explicitly impose the continuity and periodicity at the array cell level. Using the analysis tool presented in Section II, the simulated EEP directivity generated by the proposed periodized version of impedance (6) is given in Fig. 4 (see "periodized chirp" label). It can be observed that the global behavior of the EEP is as desired, but the pattern is not wide enough.

C. Optimization

To improve the quality of the result, an optimization is conducted on the Fourier series coefficients of the previously proposed periodic chirp impedance using the *fminsearch* routine [35] of MATLAB [36], based on the Nelder–Mead simplex algorithm. The optimization results show that a purely sinusoidal impedance provides better results

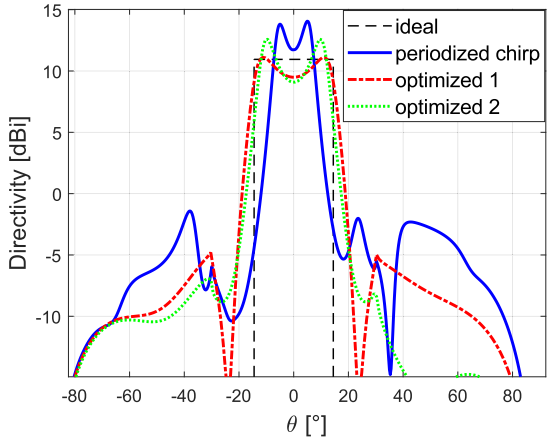

Fig. 4. Directivity of the EEP obtained with the initial periodized chirp impedance and with the two optimized sinusoidal impedances defined in (8): optimized 1 ($X_0 = -1200\ \Omega$ and $M = 1.2$) and optimized 2 ($X_0 = -900\ \Omega$ and $M = 1.3$).

than the chirp as soon as the average reactance and the modulation depth are properly adapted. The optimized impedance is given by

$$Z_s(x) = jX_0\left(1 + M\sin\left(3\frac{2\pi}{a}x\right)\right) \quad (8)$$

with $X_0 = -1200\ \Omega$ and $M = 1.2$. Note that, depending on the definition of the cost function and the optimization tool, slightly different solutions with similar performance may be obtained. For example, taking $X_0 = -900\ \Omega$ and $M = 1.3$ provides also comparable performance. Fig. 4 compares the EEP directivity given by the periodized chirp impedance with the two optimized solutions. As can be seen, a significant improvement is achieved after optimization at the cost of an unusually high modulation depth ($M > 1$). The optimized reactance is antisymmetric, thus enabling broadside radiation. Comparing the two optimized solutions, one can conclude that there is a trade-off between the flatness and the sidelobe level (SLL) of the EEP. This trade-off should be carried out according to the specifications of the desired application. In this communication, we prefer a relatively flat pattern at the expense of a slightly higher SLL. Therefore, in upcoming analyses, the design with $X_0 = -1200\ \Omega$ and $M = 1.2$ will be used.

D. Physical Interpretation

To acquire a better intuition for the radiation mechanism of the optimized impedance profile, we compared the pattern obtained when only the right half part (with respect to the reference feed) of the MTS is excited with that obtained after exciting the left half part only. The results are provided in Fig. 5. As can be seen, the left MTS part mainly contributes to the right-side pattern, and the right one contributes to the left-side pattern, which denotes a backward leaky wave radiation. The high modulation depth enables a significant leakage that helps to enlarge the pattern. Note that in the case of a sinusoidal modulation, the array cell size a should be a multiple of the impedance periodicity b (e.g., $a = 3b$ in this case) so as to also impose a periodicity at the array cell level. This observation allows one to simplify the design procedure by only selecting the odd periodicity of the impedance that will generate a -1 field harmonic [34] near the edges of the desired radiation sector. Then, the average impedance X_0 and the modulation depth M can be optimized to reach the best performance. The same methodology can be applied for other cell sizes, but it becomes more challenging to obtain a flat and sharp pattern in the desired radiation sector for smaller cell sizes,

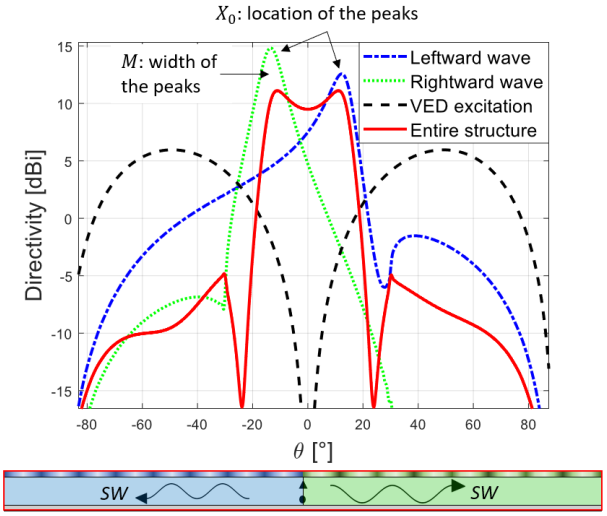

Fig. 5. EEP is the sum of three contributions: the current propagating in the right half part of the MTS, the current propagating in the left half part of the MTS, and the direct radiation of the VED excitation.

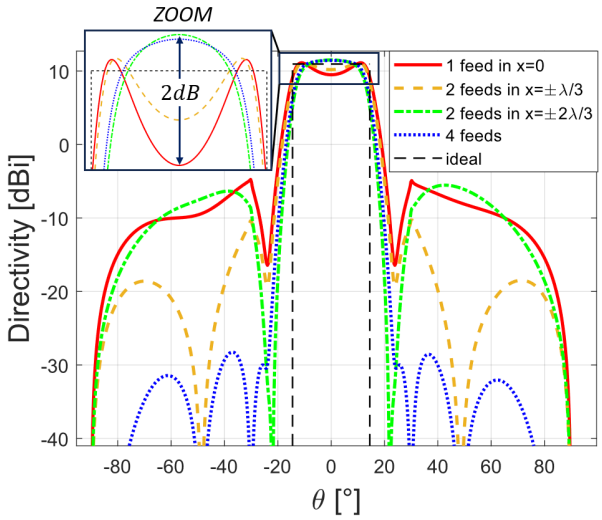

Fig. 6. EEP directivity for different feed configurations: one unitary feed located at $x = 0$, two unitary subfeeds located at $x = \pm\,\lambda/3$ and $x = \pm\,2\lambda/3$, and four subfeeds of amplitudes $A = [0.5, 1, 1, 0.5]$ located at $x = [-\lambda, -\lambda/3, \lambda/3, \lambda]$.

as the field of view is larger and the number of degrees of freedom in the impedance profile is smaller. In that case, further optimization with impedances that are not necessarily sinusoidal may be required. This aspect will be investigated in the future. Regarding the quality of the obtained EEP in Fig. 4, we observe that the transitions at the edges of the radiation sector are very sharp; as desired, the level of the sidelobes is 15.92 dB below the maximum directivity, and there is a drop of 1.62 dB (with respect to the maximum directivity) at broadside. Improving the flatness of the pattern may be achieved with a more advanced feeding design.

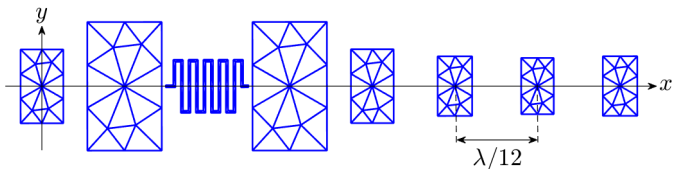

Fig. 7. Meshed patches used for implementing one $2\lambda/3$ period of the MTS (along x): rectangular patches (capacitive) and meander lines (inductive) of varying sizes.

E. Feed Configuration

This section shows how an appropriate configuration of the feed can help to improve the antenna performance. The key is to take advantage of the periodic aspect of the impedance profile. As the actual periodicity of the sinusoidal impedance is $2\lambda/3$, any translation of the feed by a multiple of $\lambda/3$ will have no impact on the amplitude of the EEP. The idea is, hence, to use a passive array of subfeeds within each cell. The subfeeds inside each passive array are fed with the same phase so as to improve the gain at broadside and, thus, reduce the drop observed in the EEP at broadside. Note that this passive array feeder spacing will not increase the number of needed active ports, because the active phase shift is applied only between consecutive cells. The subfeeds within a cell can, for instance, be realized with a corporate feeding network. Therefore, there is still a large reduction of the density of electronic components, as compared with classical phased arrays. Many feeder configurations can be envisaged, and each of them will lead to a specific EEP. As an illustration, the three following subfeed configurations (defined on the reference cell) will be selected: two unitary subfeeds located at $x = \pm\lambda/3$, two unitary subfeeds located at $x = \pm 2\lambda/3$, and four subfeeds of amplitudes $A = [0.5, 1, 1, 0.5]$ located at $x = [-\lambda, -\lambda/3, \lambda/3, \lambda]$. The amplitudes for the four subfeeds case have been chosen, so that all the subfeeds have a unitary amplitude when scanning at broadside. This design would require a combiner for subfeeds located at the edges of the array cell, since they receive power from active sources located in two consecutive cells. So, the use of four subfeeds somehow corresponds to a limit case at the boundary with overlapped subarrays. The actual design of the feeding networks is beyond the scope of this communication. The EEPs simulated with those three feeding techniques are shown in Fig. 6. We can conclude that the passive array feed design significantly impacts the EEP. In particular, we clearly observe a reduction (or disappearance) of the drop at broadside, a reduction of the SLL, and a flatter pattern. Depending on the selected feed design, a compromise can be found among feeder complexity, SLL, pattern sharpness, and/or flatness with regard to the specificities of the application.

F. Full-Wave Validation of the MTS

The synthesized impedance profile with $X_0 = -1200\ \Omega$ and $M = 1.2$ is now implemented with subwavelength patches following a procedure similar to the one used in [5]. Capacitive impedances have been implemented with rectangular patches, and the inductive ones are realized with meander lines [37]. It is worth mentioning that although the literature on SW MTSs usually assumes a capacitive sheet impedance for TM excitation [4], [5], an inductive sheet impedance can support a TM SW as long as the SW wavenumber is large enough. The patches are meshed with well-known Rao–Wilton–Glisson (RWG) basis functions [38] and are arranged in a Cartesian rectangular grid of size $\lambda/12$ along x and $\lambda/7$ along y ($\lambda = 1.25$ cm is the wavelength at 24 GHz). The meshed patches used for implementing one $2\lambda/3$ period of the MTS (along x) are shown in Fig. 7. The MTS antenna size is fixed to 14λ along x and 5λ along y. In order to emulate feeds invariant along y, each subfeed at a given position x is realized with an array of 21 VEDs placed in the middle of the substrate and arranged with $\lambda/4$ spacing along the y-direction. The EEP is computed for excitation of the center cell. The simulation is carried out with an in-house MoM solver exploiting the block-Toeplitz structure of the MoM matrix. The latter has already been validated against commercial software in [39] and [29]. The simulation results are shown in Fig. 8 for the case

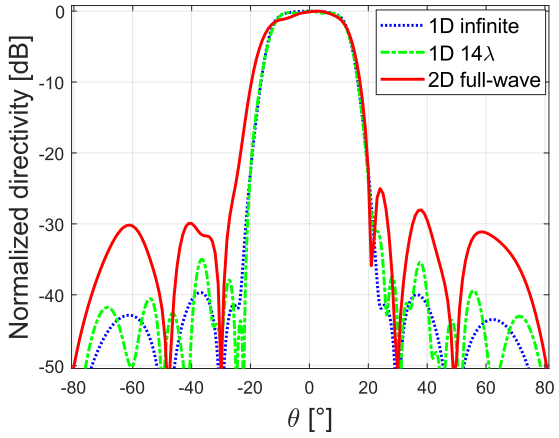

Fig. 8. EEP normalized directivity for the design with four subfeeds, for three cases: 1-D MTS of infinite length, 1-D MTS of length 14λ, and full-wave simulation of a 2-D MTS of size $14\lambda \times 5\lambda$.

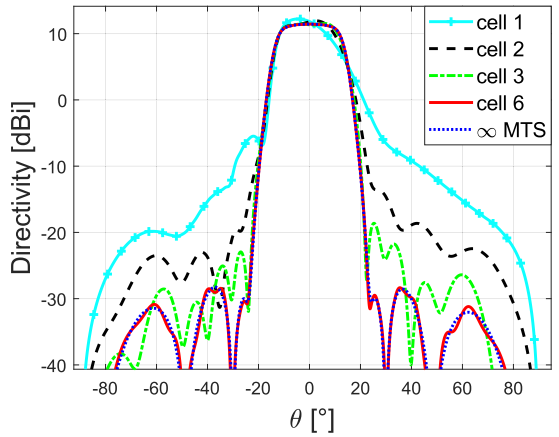

Fig. 9. EEP directivity for excitation at different cells, for an antenna of length 22λ (11 cells, cell 6 is the center cell) with four subfeeds per cell, compared with the EEP obtained for a MTS of infinite length.

of four subfeeds per cell. The normalized EEP from the full-wave simulation of the physical structure of the MTS is compared with that from the surface impedance analysis. As the directivity is defined differently for 2-D and 3-D problems, results have been normalized to ease the comparison between both cases. A very good agreement is observed, thereby proving the practical realizability of the MTS.

IV. Performance Analysis

This section aims at evaluating the performance of the scanning antenna developed in Section III. In particular, the impact of array truncation (from infinite to finite antenna) and the bandwidth of the antenna will be closely analyzed. The MTS is modulated using a sheet impedance given by (8), with $X_0 = -1200\ \Omega$ and $M = 1.2$.

A. Impact of Array Truncation

To analyze the impact of the array truncation, we consider an antenna of length 22λ (i.e., realized with 11 cells), with the set of parameters retained above (2-D analysis), and for the feed configuration with four passive subfeeds per cell (see Section III-E). The EEPs for cell feeders located in the left half of the antenna are simulated and provided in Fig. 9. As expected, the EEP of the middle cell feeder (cell 6) matches well with the infinite array prediction. However the EEP deteriorates, as the feed gets closer to the rim of the antenna, because the infinite array assumption is no longer valid. A similar behavior is observed for cell feeders located in the

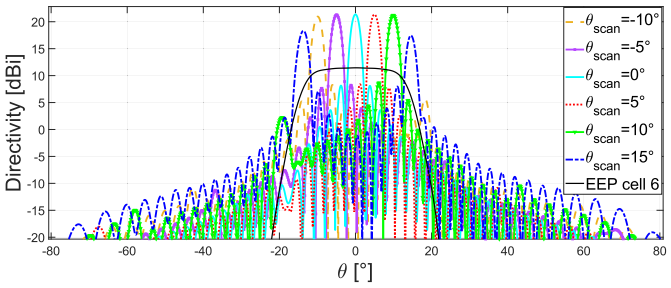

Fig. 10. MTS array pattern for various scanning directions θ_{scan}, for an antenna of length 22λ (11 cells) with four subfeeds per cell.

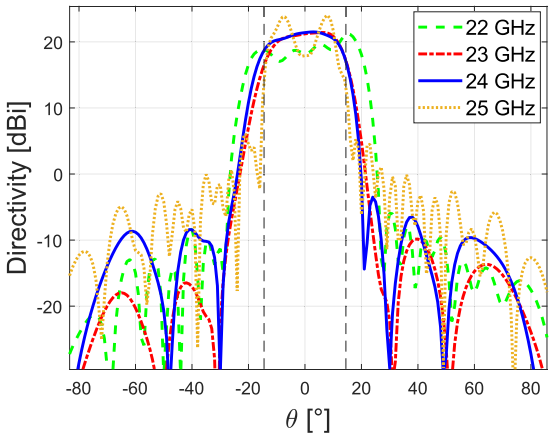

Fig. 11. 2-D full-wave simulation of the impact of the frequency on the EEP of a finite MTS of size $14\lambda \times 5\lambda$ with four subfeeds per cell. The black dashed lines correspond to the edges of the ideal rectangular EEP at 24 GHz.

right half of the antenna. Cells close to the edges may be optimized to better account for edge effects. Nevertheless, we have observed that this final optimization is not really necessary. Indeed, the ability of the finite antenna to perform scanning is illustrated in Fig. 10. The scanned beam is computed after imposing a phase shift $-\psi$ between consecutive array cells and using the EEP of each feed, taking into account the finite size of the antenna. The EEP of the feed in the center cell is superimposed on the graph to ease understanding. It can be observed that a scan range of $+/-10°$ with 15-dB grating lobe suppression is achieved. The observed scan losses are due to the EEP shapes associated with each excitation. Note that a similar behavior but with higher SLLs can be obtained with two subfeeds per cell. Therefore, a compromise should be made between feeding complexity and scanning performance.

B. Pattern Bandwidth of the Antenna

To analyze the antenna pattern bandwidth, the EEPs are simulated at different frequencies with the full-wave analysis of the physical structure of the MTS (i.e., with printed patches; see Section III-F). This analysis tool accounts for the sheet impedance variation versus frequency and the edge effects. The EEPs are shown in Fig. 11 for the case of four subfeeds per cell. It can be observed that the obtained EEP directivity is better in terms of SLLs and flatness of the pattern at 23 GHz than at 25 GHz, leading to a nonsymmetric behavior of the pattern bandwidth with respect to the frequency. Defining the operating frequency limits as the frequencies at which a 3-dB difference with respect to the reference pattern (at 24 GHz) is observed at any position in the radiation sector, it can be concluded that our antenna operates on a bandwidth of the order of 5%. It is worth mentioning that this bandwidth is sufficient for many applications, such as frequency modulated continuous-wave (FMCW) radars and base station antennas. Upon finer feed implementation, an active

impedance analysis will be carried out, both versus frequency and scan angle [40], [41].

V. Conclusion

A sparse-array MTS for beam-scanning applications has been proposed. The antenna combines the advantages of MTSs (low profile including the feeder, low cost, low-power losses, and so on) with that of phased arrays (continuous scanning), while providing a high gain and an operating bandwidth of the order of 5%. The sparsity of the array (2λ spacing between elements in the provided examples) is the essential improvement with respect to classical phased arrays. The latter requires a maximum spacing of $\lambda/2$ between cells to avoid grating lobes/ambiguity. In this communication, the grating lobes have been filtered out owing to a proper design of the MTS along with its feeding points. It is worth mentioning that the increase of the array cell size, and consequently the simplification of the electronics, comes with a reduction of the field of view. Therefore, this antenna technology is particularly useful for applications, such as surveillance of lanes, spotlight SAR, and sectorized base stations, where scanning with a high-gain beam is required over a 5°–50° field of view using a cheap and low-profile hardware.

References

[1] B. H. Fong, J. S. Colburn, J. J. Ottusch, J. L. Visher, and D. F. Sievenpiper, "Scalar and tensor holographic artificial impedance surfaces," *IEEE Trans. Antennas Propag.*, vol. 58, no. 10, pp. 3212–3221, Oct. 2010.

[2] G. Minatti, S. Maci, P. De Vita, A. Freni, and M. Sabbadini, "A circularly-polarized isoflux antenna based on anisotropic metasurface," *IEEE Trans. Antennas Propag.*, vol. 60, no. 11, pp. 4998–5009, Nov. 2012.

[3] M. Bodehou, A. Guth, K. A. Khalifeh, D. Heberling, and C. Craeye, "Multi-feed metasurface antennas: Direct numerical design and experimental validations," *IEEE Access*, vol. 11, pp. 35754–35762, 2023.

[4] G. Minatti, F. Caminita, E. Martini, M. Sabbadini, and S. Maci, "Synthesis of modulated-metasurface antennas with amplitude, phase, and polarization control," *IEEE Trans. Antennas Propag.*, vol. 64, no. 9, pp. 3907–3919, Sep. 2016.

[5] M. Bodehou, K. A. Khalifeh, S. N. Jha, and C. Craeye, "Direct numerical inversion methods for the design of surface wave-based metasurface antennas: Fundamentals, realizations, and perspectives," *IEEE Antennas Propag. Mag.*, vol. 64, no. 4, pp. 24–36, Aug. 2022.

[6] M. A. Francavilla, E. Martini, S. Maci, and G. Vecchi, "On the numerical simulation of metasurfaces with impedance boundary condition integral equations," *IEEE Trans. Antennas Propag.*, vol. 63, no. 5, pp. 2153–2161, May 2015.

[7] D. González-Ovejero and S. Maci, "Gaussian ring basis functions for the analysis of modulated metasurface antennas," *IEEE Trans. Antennas Propag.*, vol. 63, no. 9, pp. 3982–3993, Sep. 2015.

[8] M. Bodehou, C. Craeye, H. Bui-Van, and I. Huynen, "Fourier–Bessel basis functions for the analysis of elliptical domain metasurface antennas," *IEEE Antennas Wireless Propag. Lett.*, vol. 17, pp. 675–678, 2018.

[9] J. Cavillot, M. Bodehou, S. Hubert, and C. Craeye, "Efficient analysis of planar, arbitrarily shaped, and (Bi)-anisotropic metasurface antennas," *IEEE Trans. Antennas Propag.*, vol. 70, no. 1, pp. 536–546, Jan. 2022.

[10] D. González-Ovejero, G. Minatti, G. Chattopadhyay, and S. Maci, "Multibeam by metasurface antennas," *IEEE Trans. Antennas Propag.*, vol. 65, no. 6, pp. 2923–2930, Jun. 2017.

[11] M. Bodehou, E. Martini, S. Maci, I. Huynen, and C. Craeye, "Multibeam and beam scanning with modulated metasurfaces," *IEEE Trans. Antennas Propag.*, vol. 68, no. 3, pp. 1273–1281, Mar. 2020.

[12] T. Sleasman et al., "Experimental synthetic aperture radar with dynamic metasurfaces," *IEEE Trans. Antennas Propag.*, vol. 65, no. 12, pp. 6864–6877, Dec. 2017.

[13] A. Pitilakis et al., "A multi-functional reconfigurable metasurface: Electromagnetic design accounting for fabrication aspects," *IEEE Trans. Antennas Propag.*, vol. 69, no. 3, pp. 1440–1454, Mar. 2021.

[14] S. C. Pavone, E. Martini, F. Caminita, M. Albani, and S. Maci, "Surface wave dispersion for a tunable grounded liquid crystal substrate without and with metasurface on top," *IEEE Trans. Antennas Propag.*, vol. 65, no. 7, pp. 3540–3548, Jul. 2017.

[15] G. M. Rebeiz et al., "Millimeter-wave large-scale phased-arrays for 5G systems," in *Proc. IEEE MTT-S Int. Microwave Symp.*, May 2015, pp. 1–3.

[16] R. T. Maximidis, D. Caratelli, G. Toso, and A. B. Smolders, "Design of overlapped subarrays based on aperture reactive loading," *IEEE Trans. Antennas Propag.*, vol. 68, no. 7, pp. 5322–5333, Jul. 2020.

[17] C. Dragone, "A periodic array with a nearly ideal element pattern," U.S. Patent EP 0 430 516 A2, Jun. 1, 1991.

[18] S. P. Skobelev, "On the ideal element pattern in planar phased array antennas," in *Proc. IEEE Antennas Propag. Soc. Int. Symp. Dig. Held Conjunct with: USNC/CNC/URSI North Amer. Radio Sci. Meeting*, vol. 2, Jul. 2003, pp. 444–447.

[19] S. P. Skobelev, *Phased Array Antennas With Optimized Element Patterns*. Norwood, MA, USA: Artech House, 2011.

[20] P. Shelton, "Multiple-feed systems for objectives," *IEEE Trans. Antennas Propag.*, vols. AP-13, no. 6, pp. 992–994, Nov. 1965.

[21] R. Mailloux, *Phased Array Antenna Handbook*, 2nd ed., Norwood, MA, USA: Artech House, 2005.

[22] R. J. Mailloux, "Constrained feed techniques for phased array subarrays," U.S. Patent 6 549 171 B1, Apr. 5, 2003.

[23] S. P. Skobelev, "Methods of constructing optimum phased-array antennas for limited field of view," *IEEE Antennas Propag. Mag.*, vol. 40, no. 2, pp. 39–50, Apr. 1998.

[24] S. Lin, Y. Ge, and Z. D. Chen, "Grating lobe reduction in sparse arrays with a metasurface lens," in *Proc. Cross Strait Radio Sci. Wireless Technol. Conf. (CSRSWTC)*, Oct. 2021, pp. 92–94.

[25] Y. Ge, Z. Wang, J. Chen, S. Lin, and Z. Chen, "Large-spacing array antenna grating lobe suppression technology based on metamaterial lens," CN Patent 115 863, Mar. 4, 2023.

[26] P. Wang and J. Liu, "Fabry–Perot cavity structural type large-spacing phased array antenna," CN Patent 116 706, Sep. 6, 2023.

[27] A. Edalati and T. A. Denidni, "Experimental investigation of a new reconfigurable sectoral antenna," in *Proc. IEEE Antennas Propag. Soc. Int. Symp.*, Jul. 2010, pp. 1–4.

[28] A. Moreira, P. Prats-Iraola, M. Younis, G. Krieger, I. Hajnsek, and K. P. Papathanassiou, "A tutorial on synthetic aperture radar," *IEEE Geosci. Remote Sens. Mag.*, vol. 1, no. 1, pp. 6–43, Mar. 2013.

[29] J. Cavillot, M. Bodehou, and C. Craeye, "Metasurface antennas design: Full-wave feeder modeling and far-field optimization," *IEEE Trans. Antennas Propag.*, vol. 71, no. 1, pp. 39–49, Jan. 2023.

[30] L. C. Trintinalia and H. Ling, "Integral equation modeling of multilayered doubly-periodic lossy structures using periodic boundary condition and a connection scheme," *IEEE Trans. Antennas Propag.*, vol. 52, no. 9, pp. 2253–2261, Sep. 2004.

[31] X. Dardenne and C. Craeye, "Method of moments simulation of infinitely periodic structures combining metal with connected dielectric objects," *IEEE Trans. Antennas Propag.*, vol. 56, no. 8, pp. 2372–2380, Aug. 2008.

[32] J. Dessy, M. Bodehou, and C. Craeye, "Method of moments for the two-dimensional analysis of array-fed metasurface antennas," presented at Int. Conf. Electromagn. Adv. Appl. (ICEAA), May 2024.

[33] M. Bodehou, C. Craeye, E. Martini, and I. Huynen, "A quasi-direct method for the surface impedance design of modulated metasurface antennas," *IEEE Trans. Antennas Propag.*, vol. 67, no. 1, pp. 24–36, Jan. 2019.

[34] A. Oliner and A. Hessel, "Guided waves on sinusoidally-modulated reactance surfaces," *IRE Trans. Antennas Propag.*, vol. 7, no. 5, pp. 201–208, Dec. 1959.

[35] (2020). *MATLAB*. [Online]. Available: https://www.mathworks.com/help/MATLAB/ref/fminsearch.html

[36] *MATLAB*, MathWorks, Inc., Natick, MA, USA, 2022.

[37] J. Budhu, L. Szymanski, and A. Grbic, "Design of planar and conformal, passive, lossless metasurfaces that beamform," *IEEE J. Microwave*, vol. 2, no. 3, pp. 401–418, Jul. 2022.

[38] S. Rao, D. Wilton, and A. Glisson, "Electromagnetic scattering by surfaces of arbitrary shape," *IEEE Trans. Antennas Propag.*, vols. AP-30, no. 3, pp. 409–418, May 1982.

[39] H. V. Bui, S. N. Jha, and C. Craeye, "Fast full-wave synthesis of printed antenna arrays including mutual coupling," *IEEE Trans. Antennas Propag.*, vol. 64, no. 12, pp. 5163–5171, Dec. 2016.

[40] C. Hansen, *Phased Array Antennas*. Hoboken, NJ, USA: Wiley, Dec. 2009.

[41] C. Craeye and D. González-Ovejero, "A review on array mutual coupling analysis," *Radio Sci.*, vol. 46, no. 2, pp. 1–25, Apr. 2011.